762045

Groundwater flow and geochemistry in the southeastern San Juan Basin: Implications for microbial transport and activity

Water Resources Research

(Submitted: July, 1998)

Michelle A. Walvoord[1], Page Pegram[1,2], Fred M. Phillips[1], Mark Person[3], Thomas L. Kieft[4], James K. Fredrickson[5], James P. Mc Kinley[5], John Swenson[3]

[1]Earth & Environmental Science Department, New Mexico Institute of Mining and Technology, Socorro, New Mexico, 87801.

[2]Now at Daniel B. Stephens & Associates, Albuquerque, New Mexico, 87109.

[3]Department of Geology and Geophysics, University of Minnesota, Minneapolis, Minnesota, 55455.

[4]Department of Biology, New Mexico Institute of Mining and Technology, Socorro, New Mexico, 87801.

[5]Pacific Northwest National Laboratories, 902 Battelle Blvd., Richland, Washington, 99352.

Submitted July 1998
Accepted Jan. 1999

DISCLAIMER

)nfirmation of microorganisms in the deep subsurface has raised questions as to whether microbes
sported to their current residence from the surface or have been surviving in situ since sediment
ı. To address these and related questions, we characterized the microbiology and hydrogeology
Cretaceous sandstone and shale sequence in the southeastern San Juan Basin, New Mexico near a
olcanic intrusion. Deep core samples were analyzed for microbial activity to assess
tion of the previously sterilized zone around the intrusion. Groundwater geochemistry and
ta from 11 wells were used to improve our understanding of the flow regime. We modeled the
al evolution from the recharge area to each sample location and corrected ^{14}C activities for
)on inputs. The ^{14}C ages provided the basis for calibrating a cross-sectional flow model that
ıe intrusion. Hydrogeologic modeling results were consistent with microbial activity data that
ıd sufficient time to recolonize the previously sterilized region through advective transport.
upward groundwater flow near the intrusion and high vertical hydraulic conductivities for
t considerable hydraulic connection between lithologic units, which may influence the nutrient
ınd promote enhanced microbial activity near lithologic interfaces.

Introduction

Investigations over the past ten years have established that the biosphere extends deep into the terrestrial subsurface, i.e., that indigenous microorganisms live in rocks and sediments at depths up to 4 km below the earth's surface [*Ghiorse and Balkwill*, 1983; *Ghiorse and Wilson*, 1988; *Stevens et al.*, 1993; *Madsen and Ghiorse*, 1993; *Pedersen*, 1993; *Fredrickson et al.*, 1991, 1995]. Physical and chemical properties of the subsurface control the abundance and types of microorganisms present [*Kieft et al.*, 1993, 1995; *Chapelle*, 1993; *Madsen and Ghiorse*, 1993; *Fredrickson et al.*, 1989; *Stevens and McKinley*, 1995]. However, the origins of these microorganisms are generally unknown. Two hypotheses, not mutually exclusive, can explain the origins of subsurface microbes: 1) that microorganisms have survived within subsurface rocks or sediments since the time of geologic deposition (in situ survival hypothesis), and 2) that subsurface microorganisms have been transported from the surface since the time of geologic deposition (transport hypothesis) [*Murphy et al.*, 1992]. Depending on hydrogeological conditions, one or both hypotheses may be invoked. One approach for addressing these hypotheses is to identify a study site in which in situ survival or microbial transport can be constrained.

Such a site was chosen in the San Juan Basin of northwestern New Mexico. It consisted of a sequence of alternating Cretaceous sandstones and shales that was intruded by a volcanic neck, Cerro Negro, at 3.39 Ma [*Hallett et al.*, 1997]. Cores were collected for microbiological, geochemical, and physical analyses from boreholes drilled at two adjacent locations. The first of these, a vertical borehole, was intended to be far enough away from the volcanic neck that the strata would not have been impacted by the heat from volcanism. The second borehole was drilled at an angle directed toward the intrusion in order to sample along the paleo-thermal gradient. The geologic constraints based on an assumption of localized sterilization due to heating associated with the volcanic intrusion provided a basis for evaluating the relative contributions of transport and in situ survival to the microbial community structure at this site. A microbial transport origin would be supported if microbes could be found in previously heated sediments near the intrusion, i.e. within the paleo-thermal aureole. Alternatively, if microbes were absent near the intrusion, this would suggest that microbial transport was insufficient to recolonize the sterilized zone. An

survival origin would be supported by the existence of microbes exclusively outside of the paleo-
al aureole. The study site also enabled examination of microbial abundance and activities at
sandstone interfaces. *McMahon and Chapelle* [1991] have hypothesized that alternating shale and
one layers provide contrasts in electron acceptors and donors that are favorable for microbial
olism and hence encourage high microbial activity near the lithologic interfaces.

jective of this study was to provide a hydrogeologic context for testing the microbial origins
ses and for understanding the cross-strata migration of nutrients. Groundwater flow patterns and
es can establish the potential for microbial transport and provide an estimate of nutrient fluxes.
eologic and geochemical data, and results from reaction path geochemical modeling and ^{14}C dating
egrated into a 2-dimensional groundwater flow model. The model served as a tool for better
nding the hydrologic regime of the southeastern San Juan Basin and also provided quantification of
ater flow rates.

ologic Setting

site is located within the southeastern San Juan Basin, New Mexico (Figure 1). The San Juan
Laramide structural depression located on the eastern margin of the Colorado Plateau [*Kelley*,
esozoic sedimentary layers crop out at the basin edges. Early Cenozoic folding followed by late
racturing and uplift resulted in minor deformation of strata in the southeastern San Juan Basin
nd Schlee, 1967]. Sedimentary layers in this area show a regional dip of about 2% to the north-
Schlee and Moench, 1963]. Faults in this area are widely spaced and of small displacement.

aphy of the study area is characterized by a layer-cake sedimentary sequence of alternating
limestones and shales of Cambrian to Tertiary age [*Molenaar*, 1977; *Stone et al.*, 1983].
salt flows extending from Mount Taylor, a 3442 m peak, to the surrounding Mesa Chivato
ap the sedimentary sequence. The sedimentary units of interest for this study are bounded on
e Cretaceous Point Lookout Sandstone and extend down to the Triassic Chinle Formation,

which overlies Paleozoic bedrock. Quaternary deposits in the San Juan Basin include alluvial valley fill and terrace deposits. All drainageways in the San Juan Basin contain alluvial deposits consisting of gravel, sand, silt and clay [*Stone et al.*, 1983]. Table 1 lists the hydrostratigraphic units considered for this study and their associated hydrogeologic properties.

The Cerro Negro volcanic neck intruded the Mesozoic sedimentary strata at 3.39 ± 0.02 Ma [*Hallett et al.*, 1997]. The elongate dike-like neck is one of the Rio Puerco necks within the Mount Taylor volcanic field, part of a broad belt of late Cenozoic volcanism marking the transition between the Rio Grande Rift and the Colorado Plateau. Cerro Negro consists of two plugs, three non-continuous dikes, and minor pyroclastic deposits that erupted through the sedimentary layers. These igneous features trend N5E . The northern peak, the larger of the two plugs, reaches an elevation of 2201 m, with an irregular basal diameter of approximately 38 m. The southern peak, located about 122 m south of the larger plug, reaches an elevation of 2147 m, with a basal diameter of 30 m. Both plugs are composed of homogeneous, non-vesicular olivine basalt. *Schlee and Moench* [1963] indicate several north to northeast trending normal faults north of Cerro Negro, showing very little displacement.

Groundwater Hydrology

In general, groundwater in the San Juan Basin moves toward the basin center from recharge areas along the southern, northeastern, and western basin margins [*Stone et al.*, 1983]. However, in the study area the direction of flow is toward the basin margin due to the topographic high of Mount Taylor located inward of the basin margin. A contoured water table elevation map was constructed using elevation measurements from 76 wells and 15 springs in the region. The water table configuration indicates that groundwater flows east-southeast from Mount Taylor to Cerro Negro (Figure 1). Depth of water varies greatly from >550 m beneath the peak of Mount Taylor to 25-70 m below Mesa Chivato.

ınd CNV-R) were drilled 1200 m southwest of the main volcanic plug
CNA-R) was drilled 450 m southwest of the intrusion at an approximately
›ody (Figure 2). The vertical and angled boreholes reached depths of 223.5
· angled borehole did not intersect the main body of the plug but did
:) basaltic dikes, suggesting close proximity to the main body.

›tary method similar to that described by *Colwell et al.* [1992]. Solute
ted hydrocarbon) and a particulate tracer (carboxlated, fluorescent, 1μm-
drilling fluids, as described by *Phelps et al.* [1989], *McKinley and*
992], to detect contamination in samples collected for microbial
(18 from the shale and 47 from the sandstone) were collected with
bcores were collected using aseptic techniques [*Fredrickson and*
: rock cores in order to avoid possible contamination from the core
al. [1992]. Immediately after coring and retrieval within disinfected
V and CNA-R were transferred into an argon-filled glove box.
of approximately 5 cm- diameter or less, and dispensed into sterile
ing jars. The jars were then removed from the inert atmosphere of
·ollaborating laboratories for analyses. Solute and particulate
ıd subcore material as previously described [*Phelps et al.*, 1989;
:*Kinley and Colwell*, 1996]. The criterion for subcore acceptance
ıcentrations of tracers between parings and subcore to identify
uid.

Microbiological ActivityAnalyses

Mineralization of ^{14}C-labeled acetate to $^{14}CO_2$ was quantified in rock slurries essentially as described by *Fredrickson et al.* [1997]. A 0.2 mL solution of sterile [1-^{14}C] sodium acetate (74 kBq µmol-1, >98% radiopurity, NEN Research Products, Boston, MA) was added along with 4.8 ml sterile artificial groundwater to 5.0 g homogenized rock in sterile 150-ml glass bottles. Artificial groundwater contained 3.8 mg NaF, 0.2 mg KBr, 7.2 mg KCl, 336.4 mg $CaCl_2 2H_2O$, 713 mg Na_2SO_4, 32.7 mg $MgCl_2 6H_2O$, 200.8 mg NaCl, 82.2 mg $Na_2SiO_3 9H_2O$, and 899.8 mg $NaHCO_3$ L^{-1} deionized water. For anaerobic assays, rock material was handled in an anaerobic glove bag and all solutions were purged with O_2-free N_2. Slurries were incubated at 22°C. Labeled CO_2 in the headspace of the bottles was trapped in an alkaline olution consisting of 1 mL 0.3 M KOH. The KOH was transferred to liquid scintillation; radioactivity vas quantified by liquid scintillation counting. Sterile subsurface samples (autoclaved on three successive ays) served as controls.

ılfate reducing activity was measured using ^{35}S-labeled sulfate, as described by *Fredrickson et al.* [1997]. rile artificial groundwater (as described above, but without the Na_2SO_4) (10 mL), a sterile solution ıtaining 20 mM each of sodium benzoate, ammonium formate, sodium lactate, propionic acid, isobutyric J, and sodium acetate (5 mL), and a $^{35}SO_4^{2-}$ solution (370 kBq, carrier-free, NEN Research Products) (1 was added to 10 g crushed rock in sterile Balsch tubes (Bellco, Vineland, NJ). All manipulations were ormed in a sterile glove bag and all solutions were purged of O_2. Samples were incubated in the dark at ı temperature for 14 days, after which Zn acetate was added and the samples were frozen. For sis, samples were centrifuged and labeled sulfate was measured in the supernatant by liquid llation counting. Total reduced ^{35}S in sediments was quantified by chromium reduction [*Canfield et* 986] and liquid scintillation counting.

dwater Sampling and Analyses

lwater samples were collected for chemical and isotopic analysis from 11 wells shown in Figure 1. d wells included those developed for domestic, irrigation, livestock watering supplies in addtion to ing wells and the vertical borehole (CNV) drilled as part of this study. Three groundwater samples

?, CNV-W5, and CNV-W3. Sampled depth
le 2. An in-line Hydrolab sonde was used to
gen during sampling. All wells were
bmersible pump, until these parameters
ositional analysis, dissolved carbon
Cations were measured by inductively
e measured by ion chromatography. All
n a Dohrmann carbon analyzer at Pacific
ere by accelerator mass spectrometry at the
ore National Laboratories (Livermore, CA).
e ^{13}C samples were extracted with
mass spectrometry at Duke University
to PDB (Pee Dee Belemnite). $\delta^{18}O$ and δD
ope Laboratory (Pullman, WA) and at New
orted stable isotope values are the means
(‰) relative to SMOW (Standard Mean
counting on electrically enriched samples
(Ontario, Canada), and are expressed in

sulfate reduction) was found in samples
was not detected in all samples,
stringers. There was no apparent
ty to the intrusion. The major pattern
stone/shale interfaces. Also, the

frequency of samples with detectable microbial activities, as well as their magnitude, was higher in the sandstones than in the shales.

Geochemistry

Results from geochemical and isotopic analyses for groundwater collected from 11 wells showed several trends in concentration with distance from Mesa Chivato (Table 3).

Anions

Bicarbonate (HCO_3^-), calculated from pH and DIC measurements, and sulfate (SO_4^{2-}) concentrations increased with distance from Mesa Chivato. These increases suggest the dissolution of carbonate minerals and gypsum and oxidation of pyrite as groundwater moves through the system. Nitrate (NO_3^-) and dissolved oxygen (DO)concentrations, and Eh values were elevated in samples taken from the wells on Mesa Chivato (Presbyterian and Elkins) as compared to downgradient wells which indicates that the environment becomes increasingly reducing with flow distance, probably due to microbial respiration. The measured DO value at L-Bar is higher than expected, which suggests that there may have been some contamination during sampling. No samples showed measurable amounts of nitrite (NO_2^-). Silica concentrations were highest in the upgradient wells, and generally decreased downgradient, probably due to the precipitation of silicate minerals. Chloride (Cl^-) concentrations were consistently low, except in the "MW" monitoring wells. These high Cl- concentrations are most likely anthropogenic in origin. The construction of the L-Bar uranium mine tailings ponds (location indicated on Figure 1), lined with sodium chloride-treated clay in the late 70s and early 80s, acted as a point source for NaCl. Ponding resulted in mounding of the water table beneath the ponds and encouraged radial migration of soluble salts to the surrounding monitoring wells.

Cations

The patterns of generally decreasing concentration in K^+, Ca^{2+}, and Mg^{2+} with distance eastward of Mesa Chivato were very similar suggesting that their sinks are the same. The CNV-W2 sample, however, was high in potassium but low in calcium and magnesium. This sample also had an unusually high ^{14}C activity

(as discussed later), indicating vertical leakage from the surface at this site. The high potassium in CNV-W2 may be a result of local water input from vertical leakage. The concentration of Na^+ increased in the direction of groundwater flow. A Piper trilinear diagram (Figure 4) illustrates the importance of cation exchange on cation composition in this flow system.

Carbon Isotopes

The ^{13}C ratio increased with distance eastward of Mesa Chivato from approximately -14 ‰ to -3 ‰, paralleling the DIC increase. Just prior to recharge, soilwater normally has a $\delta^{13}C$ value in equilibrium with that of soil CO_2, approximately -20 ‰. Dissolution of carbonate minerals, with heavier $\delta^{13}C$ values, was most likely responsible for the enrichment in $\delta^{13}C$ in the direction of flow. Carbonate samples (fossil shell, concretion, cement, and vein) in the study area show a large range of isotopic compositions from +2.2 ‰ to −11.8 ‰ (*T.C. Onstott*, unpublished data, 1995).

Carbon-14 activity decreased with distance eastward of Mesa Chivato, reaching nearly zero at the Cerro Negro vertical borehole and the L-Bar monitoring wells. Carbon-14 activity in the CNV-W2 sample was anomalously high (52.29 ± 0.37 pmc). This sample was taken at the water table from the Two Wells Sandstone in the Cerro Negro vertical borehole. Samples, CNV-W3 and CNV-W5, collected below CNV-W2 in the same borehole yielded much older corrected ^{14}C ages (> 20 kyr). The high ^{14}C activity in CNV-W2 probably resulted from vertical recharge from the surface, which introduced young water into the top of the aquifer in this area.

Tritium

Only the Elkins well, one of the recharge wells, contained detectable tritium at 0.9 TU. The low and barely detectable levels of tritium indicate that there is no post-1952 water in groundwater samples. Also, the low tritium levels provide assurance that there was no major contamination by young water during sampling.

Stable Isotopes

A local meteoric water line, $\delta D = 8\ \delta^{18}O + 12.5$, is representative of modern precipitation in northwestern New Mexico [*Vuataz and Goff*, 1986]. All modern samples analyzed in this study plot below and to the right of the local and global meteoric water lines indicating that precipitation has experienced evaporation prior to infiltration into the groundwater system. Another interesting observation is that, in general, the younger (Holocene age) samples are 1-2 ‰ enriched in $\delta^{18}O$ and up to 14 ‰ enriched in δD relative to older (Pleistocene age) samples. These relative differences in stable isotope composition correspond to about a 3°C cooler recharge temperature for older waters. Such a trend is consistent with southwestern U.S. climate change studies that indicate a wetter, colder (5°-7°C lower than present) climate in the Pleistocene [*Phillips et al.*, 1986; *Stute et al.*, 1995] although the magnitude of the calculated temperature change is less. It is important to note that altitude effects may have also affected the relative differences in isotopic composition between the collected groundwater samples if there was significant variation in recharge elevations. However, it is difficult to distinguish between the effects of climate change and recharge elevation differences on isotopic composition.

Geochemical Model

The geochemical model NETPATH [*Plummer et al.*, 1994] was used to elucidate the groundwater geochemical evolution and to compute groundwater ages. The processes responsible for the increasing trend in DIC must be identified in order to model the geochemical effects on ^{14}C activity. Although microbial activity has been found to provide important chemical and isotopic sources and sinks in some geologic settings [*Murphy et al.*, 1992; *McMahon et al.*, 1990; *McMahon and Chapelle*, 1991], for modeling purposes the impact of microbial respiration on groundwater chemical and isotopic composition was assumed to be negligible compared to the effects of carbonate dissolution. Several lines of evidence indicate that the water chemistry of inorganic carbon species at the Cerro Negro site is dominated by carbonate mineral dissolution: (1) the increase in DIC is very large (18 to 148 ppm), but, (2) the $\delta^{13}C$ increases from –14 ‰ to –3 ‰ down the flowpath, while (3) the magnitude of the DIC increase is reproduced well by the simple carbonate mass balance model, and (4) the $\delta^{13}C$ NETPATH geochemical model results (shown in the proceeding section), without microbial respiration, are in good agreement with

ed $\delta^{13}C$ of the aquifer carbonate minerals. A simple carbonate mass balance model for this case
s that the only source of carbon entering the groundwater is from dissolution of carbonate rocks
^{13}C composition of 0 ‰, and that there is no sink for carbon leaving the groundwater. Therefore,
icted DIC concentration for a downgradient sample will be the DIC concentration in the furthest
nt well (Presbyterian) multiplied by the ratio of the $\delta^{13}C$ values between the upgradient and
lient samples. This approach predicts a significant increase in DIC along the flow system
le to the observed DIC increase. Given the strong dominance of carbonate mineral dissolution, it
ible to quantify the relatively smaller inputs from microbial respiration.

I calculates the net geochemical mass-balance reactions between an initial (upgradient) water
(downgradient) water. For this study, the sample from Presbyterian well located in the recharge
sa Chivato was taken to be the initial water and compared with all other downgradient
samples. The wells sampled do not lie along a single flowline. However, all of the
recharged through Mount Taylor and flowing away from it in a radially diverging pattern
gh a similar sequence of lithologies (Figure 5). We assume that the groundwater chemistry
ng these radial flowpaths is also similar. The mass transfers simulated by the NETPATH
onstrained by the elements listed in Table 4. Possible reactive phases used by the model are
Table 4. These mineral phases were chosen because they represent the major mineral
the geologic units through which the water flows. NETPATH mass-balance calculations
amounts (in mmols/ kg) of the phases that must dissolve or precipitate to account for the
the final water. The thermodynamic validity of each precipitation/ dissolution reaction was
saturation indices calculated by WATEQF [*Plummer et al.*, 1976], a thermodynamic
del. Saturation indices for calcite, quartz, dolomite, gypsum, and albite are reported in
n order to test the accuracy of the model, the model-predicted isotopic composition of $\delta^{13}C$
the measured $\delta^{13}C$. The mineral $\delta^{13}C$ value used by NETPATH was varied until the
ater $\delta^{13}C$ matched the measured value (Table 5). The mineral $\delta^{13}C$ thus obtained varied
and –8.5 ‰ which in most cases was within the range of measured mineral $\delta^{13}C$ from

carbonate in samples near Cerro Negro (+2.2 ‰ to −11.8 ‰), supporting the model mass balance for carbon.

Geochemical Evolution

Geochemical mass balance transfers quantified by NETPATH are listed in Table 6. In general, the model indicates that calcite is the main source of carbon along flowpaths. Precipitation of dolomite is a minor sink for carbon (except in two cases where small amounts dissolve). The dissolution of large amounts of calcite forces precipitation of dolomite and gypsum (in most cases). Ion exchange of Na^+ for Ca^{2+} from the water provides the driving force for calcium dissolution. Ion exchange removes calcium and forces calcite in the aquifer matrix to dissolve. Diffusion of Na^+ and Cl^- from low permeability units (but modeled as dissolution of NaCl) is another source of Na^+. Silica is lost through precipitation of aluminosilicate minerals and quartz. Hematite is a sink for iron, while pyrite is the main source of sulfur. The aluminosilicates (potassium feldspar and albite) are less uniform in behavior, but in most cases potassium feldspar precipitates whereas albite dissolves.

Radiocarbon Dating

The modeled system was considered to be closed with respect to carbon. The ^{14}C activity and geochemistry of the sample taken from the Presbyterian well was considered to be representative of local recharge water. Sources and sinks of carbon, such as incongruent and congruent dissolution of carbonate minerals, affect the ^{14}C signal by adding old carbon with no ^{14}C or preferentially precipitating the heavier isotope which causes the sample to appear falsely old. Therefore, the measured ^{14}C activities in downgradient wells were adjusted using NETPATH to remove all ^{14}C effects resulting from all processes other than radioactive decay. The decay equation was then applied to calculate an apparent age for groundwater in each downgradient well given the NETPATH-corrected ^{14}C activity, the initial ^{14}C activity (A_0), and the half-life of ^{14}C (5730 years). For comparison, a simple carbonate dissolution model was used to correct ^{14}C activities. In this model, ^{14}C measured values are multiplied by the ratio between the DIC concentration in the initial well and the sum of the DIC concentrations in the initial and final wells to calculate a corrected ^{14}C activity. Radiocarbon ages calculated using the simple carbonate dissolution

model were virtually identical to the ages predicted by the more rigorous NETPATH model. This implies that the carbonate geochemistry of the Cerro Negro groundwater flow system is not complicated and that the influence of microbial respiration on geochemistry and isotopic signatures is relatively small. If there were major sources of inorganic carbon other than carbonate rocks (such as oxidation of methane or microbial respiration) the isotopic and chemical data used to constrain the NETPATH model would probably not have produced the same groundwater ages as the simple carbonate dissolution calculations. Table 7 lists ^{14}C groundwater ages obtained from applying 1) a simple dissolution model and 2) the NETPATH model to correct for sources and sinks of carbon. The ages represent the travel time between the recharge area (for which the chemistry of the "Presbyterian" well was considered representative) and each well downgradient. The ages range from approximately 2,200 years at the Bibo well to >38,000 years at the MW-68 well. The ages uniformly increase with distance from the initial well. NETPATH calculates a negative age for the CNV-W2 sample, because the corrected ^{14}C activity in that sample is greater than the ^{14}C activity in the recharge well. This indicates much younger water in the CNV-W2 sample relative to the initial well, probably resulting from vertical recharge through fractures near Cerro Negro.

Groundwater Flow Model

The results from the geochemical modeling and available hydrogeologic information were integrated to develop a cross-sectional groundwater flow model of the study region. The numerical model solves a system of coupled steady-state groundwater flow and heat transfer equations for a variable-density fluid described by *Smith and Chapman* [1983], *and Fogg* [1990] and *Evans and Raffensperger* [1992]. Equivalent fresh water heads, temperatures, and stream functions are solved using triangular elements which employ linear basis functions. Heat transfer and fluid flow are formally coupled through equations of state described by *Kestin et al.* [1986] which relate density and viscosity to fluid pressure and temperature. The model was calibrated using ^{14}C ages from groundwater samples. Radiocarbon ages were compared to simulated groundwater ages using a reverse particle tracking algorithm.

Location and Hydrostratigraphic Units

The 35 km model cross-section extends from the peak of Mount Taylor to approximately 12 km beyond the Cerro Negro volcanic neck parallel to the west-northwest to east-northeast groundwater flow direction (Figure 1). Cross-sectional model thickness ranges from approximately 2000 - 1000 m, west to east. Hydrostratigraphic units were chosen based on sedimentary layers which have similar hydraulic properties (Table 1). The cross-section consists of 20 discrete aquifers and aquitards including sandstone, shale, coal, basalt, and clayey siltstone. Layers range in thickness from 5 m to 440 m. Because triangular elements are used, variable thicknesses are effectively represented in the model. The basalts at the top of Mount Taylor are also represented in the model. Because the Cerro Negro volcanic neck is very small relative to the scale of the cross-section, the intrusion is not represented in the model.

Boundary Conditions

The top boundary of the cross-sectional model constitutes a specified head equal to the water table elevation and ranges from 2800 m to 1800 m, west to east. The bottom and west side boundaries are assumed to be no-flow boundaries. Prescribed no-flow along the lower boundary is reasonable due to the large permeability contrast between the sedimentary rocks and underlying crystalline Paleozoic bedrock. To the west, the vertical no-flow boundary represents the groundwater divide beneath the top of Mount Taylor. The eastern side is an open boundary for heads and stream functions. The open condition is iterative, since the imposed stream function boundary is calculated from the darcy fluxes [described in *Senger and Fogg*, 1990].

Based on deep thermal data in *Reiter et al.* [1975] from the San Juan Basin, a relatively high basal heat flow of 100 mW m^{-2} was prescribed. The top thermal boundary was a non-uniform specified temperature that was calculated for each surface node based on the local thermal lapse rate of -5.3 °C km^{-1}, the vadose zone thickness, and vadose zone geothermal gradient of 0.07°C m^{-1}. Due to the dramatic increase in vadose zone thickness toward the peak of Mount Taylor, the calculated water table temperature actually increases with elevation, counter to the lapse rate trend. The bottom and side boundaries are no-flow heat boundaries, represented as insulated walls.

Mesh and Input Parameters

The numerical mesh consisted of 3016 nodal vertices and 5748 triangular elements. Rock properties were assigned to each triangular element. These properties included porosity, hydraulic conductivity, anisotropy, bed angle, thermal conductivity, and heat capacity of the fluid and solid phases. Porosity values, obtained from published local data [*Craigg*, 1990, *Gullett*, pers. comm, 1995] and generic values [*Freeze and Cherry*, 1979], ranged from 0.085 to 0.200 (Table 1). Hydraulic conductivities ranged from 1.0×10^{-6} m s^{-1} to 1×10^{-10} m s^{-1} based on published values [*Stone et al.*, 1983; *Risser et al.*, 1984; *Hydro-Engineering*, 1981; *Stephens*, 1983] and generic rock values [*Freeze and Cherry*, 1979]. Uniform rock thermal conductivities of 2.5 W m^{-1} K^{-1} and fluid thermal conductivities of 0.63 W m^{-1} K^{-1} were prescribed. A uniform specific heat capacity of 4187 J kg^{-1} K^{-1} was a specified fluid property.

Model Calibration

The corrected ^{14}C ages of 13 groundwater samples (well locations shown in Figure 1) represented in the cross-section were used for model calibration. A reverse particle tracking algorithm, described by *Taylor and Person* [In press] was used to calculate groundwater ages at well locations for comparison with measured ages. The model delineated the pathways from ^{14}C locations backward, at a uniform time step size of 5 years, to their respective points of recharge at the water table (Figure 5). The computed travel time for the discrete water package to reach the water table corresponds to the approximate groundwater age, assuming that advection is the dominant mechanism for isotope mass transport. Analysis by *Phillips et al.* [1989] indicated that macrodispersion did not exert a significant influence on the ^{14}C distribution in the central San Juan Basin. We also assumed that dispersion is negligible compared to advection. The model was calibrated by running over 100 simulations, varying the conductivities of hydrostratigraphic units within 3 orders of magnitude higher and lower than published or typical values (given in Table 1) in order to produce the best match of observed and computed groundwater ages. The modern ^{14}C groundwater age from CNV-2 collected at the water table was not considered in the calibration. This young ^{14}C age probably reflects local recharge through fractures in the vadose zone. Observed ages given

sodium-chloride-treated clay was emplaced on top of the Mancos Shale from 1976 to 1982. Vertical leakage through the 39.6 m of Mancos Shale caused a pulse of high concentration chloride to reach the top of the underlying Two Wells Sandstone three years after tailings were first ponded. Based on the 3 year travel time, the chloride tracer pulse yielded a vertical seepage velocity of 4.2×10^{-7} m s^{-1} and a vertical hydraulic conductivity of 5.9×10^{-8} m s^{-1}. Taking into account the area of the pond and the estimated volume of groundwater contaminated in 3 years, the chloride mass balance method yielded a vertical seepage of 7.2×10^{-8} m s^{-1} and a vertical hydraulic conductivity of 1.0×10^{-8} m s^{-1}. The values obtained using chloride as a tracer are probably representative of preferential flow through vertical fractures. Vertical hydraulic conductivities of the shales used in the calibrated model, 5.9×10^{-9} m s^{-1}, represent an average of preferential flow through fractures and matrix flow.

Model Solution

The numerical solution of the calibrated model is presented graphically as contour maps of hydraulic heads, stream functions and temperatures (Figures 6,7 & 8). Predicted stream functions (Figure 7) verify that topography-driven groundwater flow dominates the hydrogeologic regime. The groundwater is recharged between the top of Mount Taylor and the top of Mesa Chivato. Discharge is focused at the base of Mesa Chivato and extends to the vicinity of Cerro Negro and L-Bar. Groundwater flow velocities vary about 2 orders of magnitude from the Mesa Chivato recharge area to the L-Bar discharge zone east of Cerro Negro (Table 8). Average flow rates near Cerro Negro in the sediment layers that were drilled for this study range from about 0.1 – 0.3 m yr^{-1}.

In order to match the distribution of ^{14}C ages, the model must simulate deeply circulating groundwater flowpaths. The validity of this flow regime can be tested independently using temperature profiles. The modeled temperature distribution, illustrated in Figure 8, shows descending cool fluids in the recharge area depress the isotherms. In the discharge area on the east side of the cross-section, ascending groundwater advects geothermal heat toward the surface and thus uplifts the isotherms. High heat fluxes of up to 125 mWm^{-2} are predicted by the model in areas of groundwater discharge. In contrast, low heat fluxes, of < 25 mWm^{-2} are predicted in recharge areas. We tested the calibration of the model by comparing measured

mperature profiles at two wells with the simulated temperature distributions. The temperature profiles om a 340 m deep well at Bibo *[Reiter*, 1974] and the 40 m CNV-R temperature profile measured as part this study [*Walvoord*, 1998] agree well with the calculated depth distributions (Figure 9). Reiter ported a geothermal gradient of 34 °C km^{-1} at Bibo, compared to the model prediction of 31°C km^{-1}. The easured geothermal gradient at CNV-R was 56 °C km^{-1} compared to the model prediction of 44 °C km^{-1}. oth wells, Bibo and CNV-R, are located in the discharge zone and have higher than average measured and odel-calculated thermal gradients. In contrast, the Presbyterian well is located in the recharge zone and as a significantly lower model-calculated thermal gradient (included in Figure 9 for comparison). The odel-predicted stream functions indicate that water discharging at CNV-R should have circulated much eeper in the system and therefore acquired and transported greater amounts of heat than the fluid scharging at Bibo. These model predictions are consistent with the measured temperature data. The vorable comparison between the measured temperature profiles and the model predicted temperature rofiles supports the accuracy of the model.

the vicinity of Cerro Negro, groundwater flow has a strong upward component through sandstone and specially shale layers. The model solution of upward flow in a region in which there is no observable scharge other than springs located just below the mesa can be rationalized if we consider the role of ighly permeable alluvial valley fill. The hydraulic conductivity of the alluvium is >5 orders of magnitude igher than underlying sediments [*Stone et al.*, 1983], and alluvial channels have been cited as principal ocations of discharge in some areas of the San Juan Basin [*Brown*, 1976; *Stone et al.*, 1983]. We ypothesize that alluvial valley fill similarly accommodates discharge in the flat region east of Mesa hivato included in the model. The upward flux of groundwater reaches the very permeable drainageways ontaining alluvial valley fill and efficiently drains laterally. Based on modeling results (particularly the nability to match observed and model-predicted groundwater ages for > 2.5 orders of magnitude nacroanistropy), thermal and head data supporting upward gradients in the vicinity of Cerro Negro *Walvoord*, 1998], and a plausible phenomenon for accommodating discharge, we believe that the alibrated solution closely approximates the actual hydrogeology of the southeastern San Juan Basin.

Discussion

Origins of Subsurface Microorganisms

Geothermal evidence expressed in clay mineralogy, $\delta^{18}O$ values of carbonates, molecular biomarkers, and fluid inclusions suggest that the sampled sequence near Cerro Negro was not subjected to a long, pervasive thermal regime greater than 75°C. However, sandstones close to the 4 basalt dikes that penetrated the angled borehole exhibited evidence of low grade, thermal metamorphism, and the shales close to the dikes had significantly higher vitrinite reflectance ratios than shales in the upper part of the angled borehole and in the vertical borehole (P. E. Long, unpublished data, 1994). We conclude that intrusions at Cerro Negro produced a short thermal pulse which would have killed microorganisms present at the time, but did not persist long enough to be recorded in several geothermal indicators. Microbial activity (^{14}C acetate mineralization and ^{35}S sulfate reduction) was detected in many core samples collected at the Cerro Negro site, including some positioned near the volcanic intrusion adjacent to basalt dikes, indicating that microbes repopulated the previously sterilized region. The most probable mechanism of microbial re-colonization would have been through advective groundwater transport. Hydrogeologic modeling results obtained from this study further support groundwater microbial transport as the agent responsible for the recolonization of these rocks, particularly the sandstones. Considerable groundwater has flowed through the thermal aureole within the 3 My since neck emplacement. Groundwater flow velocities calculated by hydrogeologic modeling permit relatively rapid microbial recolonization of the thermal aureole. Using conservative values of a 0.1 m yr^{-1} average flow rate and a 100 m thermal aureole radius, the entire sterilized zone (200 m diameter) could have been recolonized within 2,000 years after the intrusive body cooled if microbes were transported at approximately the same rate as groundwater advection. Depending on many factors, microbial transport may have exceeded groundwater advection due to anion or size exclusion effects or conversely may have been retarded due to attachment and straining. Controlling factors include, but are not limited to, cell size, cell surface properties (charge and hydrophobicity), ionic strength and pH of the groundwater, and properties of the porous medium (porosity, tortuosity, particle size and surface properties)[*Camper et al.*, 1993; *Tan et al.*, 1994]. Attachment and detachment of microbes to porous media surfaces are the most important and complex processes affecting microbial transport and are also the least understood and poorly quantified [*Tan et al.*, 1994]. For these reasons we cannot present precise time

estimates of microbial recolonization. However, given a period of 3 My, microbial retardation relative to advection would have had to exceed a linear retardation factor of 1500 to prevent repopulation of the thermal aureole. Many experimentally-determined retardation factors, both in the laboratory and in situ, are actually < 1.0 suggesting that anion and/or size exclusion is enhancing transport relative to adsorption, particularly at low flow velocities such as those near Cerro Negro [*Camper et al.*, 1993; *Harvey*, 1997]. Based on our hydrodynamic characterization of the study area and the assumption that microbial retardation was <<1500, we can confidently submit that microbial recolonization of the Cerro Negro thermal aureole was possible through groundwater microbial transport. The estimate of complete recolonization is consistent with the absence of any remnant pattern in microbiology reflecting past heating; i.e., there is no gradational trend of decreasing microbial activity with proximity to the volcanic neck.

Contrary to original expectations, microbial activity was detected in some shale samples collected near the intrusion. It was originally believed that the small porethroats of the shales would inhibit transport of microorganisms back into the previously sterilized zone. However, it is now evident that the shale contains vertical fractures that could serve as conduits for relatively rapid advection of microorganisms. *Fredrickson et al.* [1997] found little or no microbial activity in intact, unfractured shale samples but high rates in material with a significant fraction of porethroat diameters >0.2 μm. Calculations using chloride mass balance methods (at the L-Bar tailings pond, described above), and hydrogeologic modeling indicate relatively high vertical flow rates through the main body and interbeds of the Mancos Shale, confirming the importance of fracture flow. Consequently, the results of this study support the transport hypothesis for the origins of microorganisms in these Cretaceous sediments more strongly than the in situ survival hypothesis.

Microbial Activities at Shale/Sandstone Interfaces

Both physical and chemical parameters likely control the vertical distribution of microbial activity within a shale/sandstone sequence. An important physical parameter influencing microbial distribution in the subsurface is porethroat size. Minimal microbial activity measured in the shales, particularly where fracturing is absent, probably results from the significantly smaller size distribution of porethroats which

inhibits microbial growth and transport [*Fredrickson et al.*, 1997]. An important chemical parameter influencing microbial distribution is porewater geochemistry, which is governed largely by lithology. Shale, because of its relatively high organic content, is generally abundant in electron donors such as organic acids, and sandstone porewater is often abundant in electron acceptors such as sulfate. *McMahon and Chapelle* [1991] showed that diffusion of organic acids from fine-grained aquitard sediments into electron acceptor-rich coarse-grained aquifers provided an environment near the aquitard/aquifer contact that was favorable to respiratory bacteria. Within the 200 - 300 m deep package of Cretaceous shale and sandstone layers near Cerro Negro, some of the highest rates of microbial activity were measured in the upper portions of sandstone units near the shale interfaces [*Fredrickson et al.*, 1997]. *Krumholz et al.* [1997] also detected increased sulfate reduction activity in shale-sandstone interfaces in the vicinity of Cerro Negro. However, the irregularities in the microbial activity pattern within the sandstone units are not explained by the 1-dimensional nutrient diffusion hypothesis put forth by *McMahon and Chapelle* [1991]. The complexity of both the nutrient distribution and the hydrologic regime probably contribute to these patterns, and preclude a simple explanation of solute-transport-controlled microbial distribution. The distribution of sulfate, probably the most abundant electron acceptor in the anoxic portion of these sedimentary units, is not clearly correlated with lithology (*McKinley*, unpublished data, 1996). The strong upward flow in the vicinity of Cerro Negro, indicated by hydrogeologic modeling, should enhance the transport of nutrients out of the shale layers. The amount of upward advection, however, may be reduced due to water flux through shale fractures. Diffusion across sandstone-shale interfaces is also likely to be a significant mechanism for the cross-stratigraphic migration of organic nutrients. Detailed explanation of the formation-scale nutrient transport and biochemical reactions is beyond the scope of this investigation, but our results do demonstrate that strong vertical hydraulic gradients and multi-porosity create a much more complex transport/reaction scenario than the simple one-dimensional diffusion-controlled model envisioned for the interface hypothesis.

Conclusion

The synthesis of microbiological, geochemical and hydrogeologic data obtained from research completed under the Cerro Negro Microbial Origins Project suggests that groundwater plays an important role in the

microorganisms in subsurface environments by providing a medium for the transport of cells
or maintaining in situ microbial populations.

succeeded in re-colonizing a zone that was presumably sterilized following the
of a volcanic intrusion at 3.39 Ma. Calculated groundwater flow rates in the vicinity of the
ndicate relatively rapid microbial re-colonization (> 0.1 m yr^{-1} subsequent to intrusion and
ost of the associated heat) was possible through transport in groundwater. Groundwater
ates provide an approximate estimate for microbial re-colonization rates. The actual timing
n would depend on 1) the extent of the thermal aureole, 2) the cooling history of the
cted sediments, and 3) the retardation or enhancement of microbial transport relative to
city. Currently, these factors are not well-constrained. However, even assuming highly
ates of these parameters, calculated groundwater velocities far surpass rates required to
-colonization within the past 3 million years. Present-day microbial activity shows no
the paleothermal gradient imposed by the volcanic intrusion 3.39 Ma. This
sistent with the relatively high groundwater flow rates determined from geochemical
modeling that would have resulted in many pore volumes passing through the
liments near the intrusion. In hindsight, it is recognized that a similar study conducted
rilized zone might have produced results in which the paleothermal signature was
bial properties (i.e., on-going re-colonization of the thermal aureole might be
fective in situ microbial transport properties on relatively large time and spatial scales
d.

activity observed at several sandstone/shale interfaces in the Cerro Negro
dified version of the lithologic interface theory proposed by *McMahon and*
al and chemical groundwater results from this study further suggest that solute
influencing microbial activity in the sandstone units, whereas size distribution of
niting factor for microbial activity in shales, as suggested by *Fredrickson et al.*,
l strong upward advective flow through organic-rich shales and sulfate-rich

sandstones complicate solute transport processes, precluding a simple explanation of electron donor/ acceptor exchange at shale/sandstone interfaces.

This study illustrates the complexities of nutrient release, transport, and consumption in subsurface environments. Quantification will require a detailed understanding of both subsurface biogeochemistry and groundwater flow regimes.

Acknowledgments

This research was supported by the Deep Microbiology subprogram of the Subsurface Science Program, Office of Energy Research, U. S. Department of Energy (Grant no. DE-FG03-93ER-616833 (TLK and FMP)). Pacific Northwest National Laboratories is operated for the Department of Energy by the Battelle memorial Institute under contract no. DE-AC06-76RLO 1830.

References

Camper, A. K., J. T. Hayes, P. J. Sturman, W. L. Jones, and A. B. Cunningham, Effects of motility and adsorption rate coefficient on transport of bacteria through saturated porous media, *Applied and Environmental Microbiology, 59*, 3455-3462, 1993.

Canfield, D. E., R. Raiswell, J. T. Westrich, C. M. Reaves, and R. A. Berner, The use of chromium reduction in the analysis of reduced inorganic sulfur in sediments and shales, *Chem. Geol. 54*, 149-155, 1986.

Chapelle, F. H., Ground-Water Microbiology and Geochemistry, 424 pp., John Wiley & Sons, New York, 1993.

Colwell, F. S., G. J. Stormberg, T. J. Phelps, S. A. Birnbaum, J. P. McKinley, S. A. Rawson, C. Veverka, S. Goodwin, P. E. Long, B. F. Russell, T. Garland, D. Thompson, P. Skinner, and S. Grover, Innovative techniques for collection of saturated and unsaturated subsurface basalts and sediments for microbiological characterization, *J. Microbiol. Methods, 15*, 279-292, 1992.

Craigg, S. D., W. L. Dam, J. M. Kernodle, J. M., and G. W. Levings, Hydrogeology of the Dakota Sandstone in the San Juan structural basin, New Mexico, Colorado, Arizona and Utah, U.S.G.S. Hydrol. Invest. Atlas HA-720-I, 2 sheets, 1989.

Domenico, P. A., and F. W. Schwartz, Physical and Chemical Hydrogeology, John Wiley & Sons, New York, 824 pp., 1990.

Evans, D. G., and J. P. Raffensperger, On the stream function for variable-density groundwater flow, *Water Resour. Res., 28*, 2141-2145, 1992.

Fredrickson. J. K., T. T. Garland, R. J. Hicks, J. M. Thomas, S. W. Li, and S. M. McFadden, Lithotrophic and heterotrophic bacteria in deep subsurface sediments and their relation to sediment properties, *Geomicrobiol. J., 7*, 53-66, 1989.

Fredrickson, J. K., D. L. Balkwill, J. M. Zachara, S. W. Li, F. J. Brockman, and M. A. Simmons, Physiological diversity and distributions of heterotrophic bacteria in deep Cretaceous sediments of the Atlantic coastal plain, *Appl. Environ. Microbiol., 57*, 402-411, 1991.

Fredrickson, J. K., J. P. McKinley, S. A. Nierzwicki-Bauer, D. C. White, D. B. Ringelberg, S. A. Rawson, S. M. Li, F. J. Brockman, and B. N. Bjornstad, Microbial community structure and biogeochemistry of Miocene subsurface sediments: implications for long-term microbial survival, *Molecular Biol., 4*, 619-626, 1995.

Fredrickson, J. K., and T. J., Phelps, Subsurface drilling and sampling, in Manual of Environmental Microbiology, edited by C. J. Hurst, G. R., Knudsen, M. J., McInerney, L. D. Stetzenbach, and M. V. Walter, pp. 526-540, Am. Soc. for Microbiol., Washington, D. C., 1996.

Fredrickson, J. K., J. P. McKinley, B. N. Bjornstad, P. E. Long, D. B. Ringelberg, D. C. White, L. R. Krumholz, J. M. Suflita, F. S. Colwell, R. M. Lehman, T. J. Phelps, and T. C. Onstott, Pore-size constraints on the activity and survival of subsurface bacteria in a late Cretaceous shale-sandstone sequence, northwestern New Mexico, *Geomicrobiol. J., 14*, 183-202, 1997.

Freeze, R. A., and J. A. Cherry, Groundwater, Prentice-Hall, Inc., New Jersey, 604 pp., 1979.

Ghiorse, W. C. and D. L. Balkwill, Enumeration and morphological characterization of bacteria indigenous to subsurface sediments, *Dev. Ind. Microbiol., 24*, 213, 1983.

Ghiorse, W. C., and J. T. Wilson, Microbial ecology of the terrestrial subsurface, Adv. Appl. Microbiol., 33, 107-172, 1988.

Hallett, R. B., P. R. Kyle, and W. C. McIntosh, Paleomagnetic and 40Ar/39Ar age constraints on the chronologic evolution of the Rio Puerco volcanic necks and Mesa Prieta, west-central New Mexico: Implications for transition zone magmatism, *Geol. Soc. Am. Bul., 109*, 95-106, 1997.

Harvey, R. W., Microorganisms as tracers in groundwater injection and recovery experiments: a review, *FEMS Microbiology Reviews, 20*, 461-472, 1997.

Hydro-Engineering, Ground-water hydrology near the L-Bar tailings reservoir, prepared for Sohio Western Mining Company by Hydro-Engineering, Casper, Wyoming, 1981.

Kelley, V. C., Regional structure of the San Juan Basin: New Mexico Geological Society, Guidebook 1st Field Conference, 101-108, 1950.

Kernodle, J. M., G. W. Levings, S. D. Craigg, and W. L. Dam, Hydrogeology of the Gallup Sandstone in the San Juan structural basin, New Mexico, Colorado, Arizona and Utah, U.S. Geol. Surv. Hydrol. Invest. Atlas HA-720-H, 2 sheets, 1989.

Kestin, J., H. E. Khalifa, and R. J. Correia, Tables of the dynamic and kinematic viiscosity of aqueous NaCl solutions in the temperature range 20-150• C and the pressure range 0.1-35 MPa, *J. Phys. Chem. Ref. Data, 10*, 71-87, 1981.

Kieft, T. L., P. S. Amy, F. J. Brockman, J. K. Fredrickson, B. N. Bjornstad, and L. L. Rosacker, Microbial abundance and activities in relation to water potential in the vadose zones of arid and semiarid sites, *Microb. Ecol., 26*, 59-78, 1993.

Kieft, T. L., J. K. Fredrickson, J. P. McKinley, B. N. Bjornstad, S. A. Rawson, T. J. Phelps, F. J. Brockman, S. M. Pfiffner, Microbiological comparisons within and across contiguous lacustrine, paleosol, and fluvial subsurface sediments, *Appl. Environ. Microbiol., 61*, 749-757, 1995.

Krumholz, L. R., J. P. McKinley, G. A. Ulrich, and J. M. Suflita, Confined subsurface microbial communities in Cretaceous rock, *Nature, 386*, 64-66, 1997.

Lovley, D. R., and F. H. Chapelle, Deep subsurface microbial processes, Rev. Geophys., 33, 3, 365-381, 1995.

Madsen, E. L., and W. C. Ghiorse, Ground water microbiology: subsurface ecosystems processes, in Aquatic Microbiology: An Ecological Approach, edited by T. Ford, pp. 167-213, Blackwell Scientific Pub. Inc., Cambridge, MA, 1993.

McKinley, J. P., and F. S. Colwell, Application of perfluorocarbon tracers to microbial sampling in subsurface environments using mud-rotary and air-rotary drilling techniques, *J. Microb. Methods, 26*, 1-9, 1996.

McMahon, P. B. and F. H. Chapelle, Microbial production of organic acids in aquitard sediments and its role in aquifer geochemistry, *Nature, 349*, 233-235, 1991.

Moench, R. H., and J. S. Schlee, Geologic quadrangle map of the Seboyeta Quadrangle, New Mexico, U.S.G. S. Map GQ-207, 1963.

Molenaar, C. M., Stratigraphy and depositional history of Upper Cretaceous rocks of the San Juan Basin area, New Mexico and Colorado, with a note on economic resources, Guidebook, New Mexico Geol. Soc. 28th Field Conference, 159-166, 1977.

Murphy, E. M., J. A. Schramke, J. K. Fredrickson, H. W. Bledsoe, A. J. Francis, D. S. Sklarew, and J. C. Linehan, The influence of microbial activity and sediment organic carbon on the isotope geochemistry of the Middendorf aquifer, *Water Resour. Res., 28*, 723-740, 1992.

Neuzil, C., How permeable are clays and shales?, *Water Resour. Res., 30,* 145-150, 1994.

Pedersen, K., The deep subterranean biosphere, *Earth Science Reviews, 34*, 243-260, 1993.

Pegram, P., An isotopic study of ground-water flow near Cerro Negro, New Mexico, unpublished M.S. Thesis, 145 pp., New Mexico Institute of Mining and Technology, Socorro, NM, 1995.

Person, M., J. P. Raffensperger, S. Ge., and G. Garven, Basin-scale hydrogeological modeling, *Rev. Geophys., 34*, 61-87, 1996.

Phelps, T. J., C. B. Fliermans, T. R. Garland, S. M. Pfiffner, and D. C. White, Method for recovery of deep terrestrial subsurface sediments for microbiological studies, *J. Microbiol. Methods, 9*, 267-279, 1989.

Phillips, F. M., L. A. Peeters, M. K. Tansey, and S. N. Davis, Paleoclimatic inferences from an isotopic investigation of groundwater in the central San Juan Basin, New Mexico, *Quaternary Research, 26*, 179-193, 1986.

Phillips, F. M., M. K. Tansey, L. A. Peeters, S. Cheng, and A. Long, An isotopic investigation of groundwater in the San Juan Basin New Mexico: Carbon 14 dating as a basis for numerical flow modeling, *Water Resour. Res., 25*, 2259-2273, 1989.

Plummer, L. N., B. F. Jones, and A. H. Truesdell, WATEQF - A FORTRAN IV version of WATEQ, a computer program for calculating chemical equilibria of natural waters, U.S. Geol. Surv. Water Resour. Invest. Report 75-13, 61 pp., 1976.

Plummer, L. N., E. C. Prestemon, and D. L. Parkhurst, An interactive code (NETPATH) for modeling net geochemical reaction along a flowpath, U.S. Geol. Surv. Water Resour. Invest. Report 91-4169, 130 pp., 1994.

Risser, D. W., and F. P. Lyford, Water resources on the Pueblo of Laguna, West-Central New Mexico, U.S. Geol. Surv. Water Resour. Invest. Report 83-4038, 308 pp., 1983.

Reiter, M., C. L. Edwards, H. Hartman, C. Weidman, Terrestrial heat flow along the Rio Grande Rift, New Mexico and Southern Colorado, *Geol. Soc. Am. Bull., 86*, 811-818, 1975.

Schlee, J. S., and R. H. Moench, Geologic quadrangle map of the Moquino quadrangle, New Mexico, U.S. Geol. Surv. Map GQ-209, 1963.

Senger, R. K., and G. E. Fogg, Stream functions and equivalent freshwater heads for modeling regional flow of variable-density groundwater, 1. Review of theory and verification, *Water Resour. Res., 26*, 2089-2096, 1990.

Smith, L., and D. S. Chapman, On the thermal effects of groundwater flow 1. Regional scale systems, *J. Geophys. Res., 88*, 593-608, 1983.

Stephens, D. B., Ground water flow and implications for groundwater contamination north of Prewitt, New Mexico, U.S.A., *J. Hydrol., 61*, 391-408, 1983.

Stevens, T. O., J. P. McKinley, and J. K. Fredrickson, Bacteria associated with deep, alkaline, anaerobic groundwaters in southeast Washington, *Microb. Ecol., 25*, 35, 1993.

Stevens, T. O. and J. P. McKinley, Geochemically produced hydrogen supports microbial ecosystems in deep basalt aquifers, *Science, 270*, 450-454, 1995.

Stone, W. J., F. P. Lyford, P. F. Frenzel, N. H. Mizell, and E. T. Padgett, Hydrogeology and water resources of San Juan Basin, New Mexico, Hydrologic Report 6, 70 pp., New Mexico Bureau of Mines and Mineral Resources, Socorro, NM, 1983.

Stute, M., J. F. Clark, P. Schlosser, W. Broecker, and G. Bonani, A 30,000 yr continental paleotemperature record derived from noble gases dissolved in groundwater from the San Juan Basin, New Mexico, *Quaternary Research, 43*, 209-220, 1995.

Tan, Y., J. T. Gannon, P. Baveye, and M. Alexander, Transport of bacteria in an aquifer sand: Experiments and model simulations, *Water Resour. Res., 30*, 3243-3252, 1994.

Taylor, J. Z. and M. Person, Wellhead delineation on island aquifer systems, *Groundwater*, accepted, 1998.

Vacquier, V., The origin of terrestrial heat flow, *Geophys. J. Int., 106*, 199-202, 1991.

Vuataz, F. D., and F. Goff, Isotope geochemistry of thermal and nonthermal waters in the Valles Caldera, Jemez Mountains, northern New Mexico, *J. Geophys. Res., 92*, 2, 1835-1853, 1986.

Walvoord, M., Characterization of groundwater flow in the southeastern San Juan Basin: Implications for microbial origins in the deep subsurface near Cerro Negro, New Mexico, unpublished M.S. Thesis, 143 pp., New Mexico Institute of Mining and Technology, Socorro, NM, 1998.

Figure 1. Location of study area in northwestern New Mexico (bottom left); Water table elevation contours (solid lines; in meters) with groundwater sample locations (bullets) are included. A-A' designates the cross-section represented by the model (upper right).

Figure 2. Stratigraphy and orientation of boreholes drilled near the Cerro Negro volcanic neck.

Figure 3. Microbial activity measurements (total reduced $^{35}SO_4^{2-}$ and ^{14}C mineralization) with depth in the CNA-R borehole. The locations of basaltic stringers are noted. In general, higher activities were observed near the sandstone/shale interfaces. Total reduced $^{35}SO_4^{2-}$ and ^{14}C mineralization measurements taken from the vertical borehole (not presented here) showed similar trends, although activities were lower.

Figure 4. Piper trilinear diagram. The areas of the circles plotted on the central field are porportional to total dissolved solid concentrations for each water sample.

Figure 5. Cross-sectional groundwater flow model, taken from A – A', with well locations and pathlines recorded from reverse particle-tracking. The top boundary represents the water table.

Figure 6. Calculated heads (in m) along cross-sectional transect from Mt. Taylor to east of the Cerro Negro intrusion.

Figure 7. Calculated stream functions (in $m^2\ yr^{-1}$) along cross-sectional transect from Mt. Taylor to east of the Cerro Negro intrusion.

Figure 8. Calculated temperatures (in °C) along cross-sectional transect from Mt. Taylor to east of the Cerro Negro intrusion.

Figure 9. Comparison of measured and model-calculated temperature profiles from wells located along the A-A' cross-section in the discharge zone and recharge zone. Curvature in observed and modeled temperature profiles are primarily due to vertical groundwater flow and associated convective heat transfer.

Unit	Thickness (m)	Porosity (%)	Kx values (m/s)	Kz values (m/s)	Kx used in calibrated model [m/s]	Kz used in calibrated model [m/s]
Alluvium	>40		$10^{-5} - 10^{-2}$ (5)			
Basalt	0-545	10 (1)	$10^{-11} - 10^{-7}$ (1)		3.2×10^{-9}	3.2×10^{-9}
Point Lookout Sandstone	35-40	20 (2)	3.2×10^{-8} (5)		5.1×10^{-8}	5.1×10^{-8}
Satan Tongue of the Mancos Shale	5-10	12 (1)		$10^{-13} - 10^{-9}$ (1)	5.9×10^{-9}	5.9×10^{-9}
Hosta Tongue of the Point Lookout Sandstone	27-35	12 (1)	3.5×10^{-8} (5)		5.1×10^{-7}	5.1×10^{-8}
Gibson Coal Member of Crevasse Canyon	92-118	20 (3)	$< 3.2 \times 10^{-7}$ (5)		1.6×10^{-7}	1.6×10^{-8}
Dalton Sandstone Member of the Crevasse Canyon	18-28	20 (1)	3.2×10^{-7} (5)		5.1×10^{-7}	5.1×10^{-8}
Mulatto Tongue of the Mancos Shale	68-89	12 (1)		$1\text{-}5.9 \times 10^{-8}$ (9)	5.9×10^{-9}	5.9×10^{-9}
Dilco Coal Member of the Crevasse Canyon	30-48	20 (3)	$< 3.2 \times 10^{-7}$ (5)		1.0×10^{-7}	1.0×10^{-8}
Gallup Sandstone	20-25	15 (1)	9.1×10^{-7} (5)		1.9×10^{-7}	3.2×10^{-8}
Mancos Shale (main body)	20-180	12 (4)		1.0×10^{-10} (6)	5.9×10^{-9}	5.9×10^{-9}
Two Wells Sandstone	13-37	15 (4)	$< 1.3 \times 10^{-6}$ (5) $10^{-5} - 10^{-8}$ (7)		2.2×10^{-7}	2.2×10^{-8}
Whitewater Arroyo Shale	20-25	9 (4)		$10^{-13} - 10^{-9}$ (1)	5.9×10^{-9}	5.9×10^{-9}
Paguate Sandstone	20-22	8.5 (4)	$< 1.3 \times 10^{-6}$ (5)		2.1×10^{-7}	2.1×10^{-8}
Clay Mesa Shale of the Mancos Shale	8-15	10 (1)		$10^{-13} - 10^{-9}$ (1)	5.9×10^{-9}	5.9×10^{-9}
Cubero Sandstone and Oak Canyon Member	43-48	15 (4)	$< 1.3 \times 10^{-6}$ (5)		2.1×10^{-7}	2.1×10^{-8}
Brushy Basin Member of the Morrison Formation	52-60	10 (1)	1.2×10^{-6} (8)	$10^{-13} - 10^{-9}$ (1)	1.0×10^{-7}	1.0×10^{-8}
Westwater Canyon Sandstone Member	62-68	20 (1)	$< 2.7 \times 10^{-6}$ (5)		4.8×10^{-7}	4.8×10^{-8}
Recapture Shale Member	175-218	10 (1)		$10^{-13} - 10^{-9}$ (1)	5.9×10^{-9}	5.9×10^{-9}
Bluff - Cow Springs Sandstone, Summerville Formation, Todilto Limestone, and Entrada Sandstone	158-163	15 (1)	4.0×10^{-6} (5)		3.2×10^{-7}	3.2×10^{-8}
Chinle Formation	330-440	12 (1)	1.9×10^{-8} (5)	10^{-12} (10)	6.3×10^{-8}	6.3×10^{-9}

Parameter values obtained from: (1) *Domenico and Schwartz* [1990]; (2) *Craigg* [1980]; (3) *Freeze and Cherry* [1979]; (4) core sample measurements, Cheryl D. Gullett, PNNL, personal communication, 1995, (5) transmissivity values in *Stone et al.* [1983], (6) *Stephens* [1984], (7) Well tests near L-Bar Mine by Hydro-Engineering [1981], (8) SS in Brushy Basin Member by *Risser et al.* [1984], (9) Cl- tracer calculations, *Pegram* [1995], (10) *Ward et al*, [1982].

Table 1. Hydrostratigraphic units in the southeastern San Juan Basin and their associated published, generic, and model-calibrated hydraulic parameter values.

Kx – Horizontal hydraulic conductivity; Kz – Vertical hydraulic conductivity.

	Date sampled	UTM Coordinates Easting (m)	Northing (m)	Surface Elevation (m)	Water table Elevation (m)	Depth Interval (m bgs)	Screened Unit
erian	10-94	275625	3895975	2328.7	2310	19-30.0	Pt. Lookout SS
	10-94	275725	3895975	2359.7	2334.1	25.6-36.0	Pt. Lookout SS
	10-94	281429	3895320	1938.5	1879	126.5-137.2	PaguateSs
a	10-94	282401	3898401	1969.0	1870	207.3-231.6	Cubero Ss
)	10-94	284088	3894708	1891.9	1830.9	118.9-167.6	Westwater Ss
2	7-94	285438	3897475	1937.0	1875.4	139.0-144.8	Two Wells Ss
3	7-94	285438	3897475	1937.0	1875.4	194.0-199.3	Cubero Ss
5	7-94	285438	3897475	1937.0	1875.4	159.0-164.2	Paguate Ss
	5-94	386500	3896415	1895.8	1865.9	45.2-57.4	Two Wells Ss
	5-94	386500	3896750	1912.7	1866.7	65.7-78.5	Two Wells Ss
	5-94	286650	3896575	1902.0	1864.5	51.8-64.0	Two Wells Ss
	5-94	286875	3896975	1933.1	1865.5	88.3-100.5	Two Wells Ss
	10-94	288339	3896638	1875.7	1860	NA	Morrison Fm

ow ground surface; NA = information not available

Sampled well information.

Distance eastward from Mesa Chivato ⟶

Sample Name	Presb	Elkins	Bibo	Seboyeta	Moquino	CNV-W2	CNV-W3	CNV-W5	MW-64	MW-65	MW-60	MW-68	L-Bar
Temp (C)	12.5	16.0	19.7	22.9	17.7	20	20	20	19	20	19	19	18.41
pH	7.27	7.81	8.05	7.94	8.59	8.26	8.17	8.46	7.9	7.8	8.1	8.1	8.26
DO	6.87	5.91	0.62	0	0.05	0.2	0.18	0.01	-	-	-	-	2.39
Cond. (mS/cm)	0.170	0.132	0.839	0.311	0.604	0.93	0.99	1.53	-	-	-	-	1.074
Eh (mV)	395	229	273	-25	-8	282	231	233	-	-	-	-	103
DIC (ppm)	23.6	18.1	71.7	42.2	78.9	92.9	116.1	106.9	129.1	131.1	147.7	121.3	95.7
DOC (ppm)	0.78	0.67	0.66	0.75	0.71	5.29	1.84	13.85	-	-	-	-	0.86
Ca^{2+}	16.13	13.67	12.78	8.47	4.31	3.34	4.98	17.43	7.97	10.06	7.97	13	3.63
Mg^{2+}	6.42	5.2	4.73	3.23	2.29	1.35	0.77	6.61	2.83	9.77	2.83	4.47	1.32
Na^{+}	10.64	9.072	192.5	68.17	172.8	307	247.2	355.1	568.3	527.1	568.3	724.3	289.2
K^{+}	3.85	3.55	2.72	2.01	1.39	6.37	2.17	1.71	3.36	4.1	3.36	4.3	1.7
HCO_3^{-}*	119.8	91.68	362.38	213.53	393.7	464.48	585.8	535.89	653.48	664.11	746.01	612.67	482.11
F^{-}	0.17	0.19	1.03	0.23	1.57	1.85	1.38	4.53	1.53	1.81	1.84	1.71	2.15
Cl^{-}	2.7	3	15	7.8	4.1	13.9	5.3	11.2	34.2	305.4	42.6	61.4	15.1
SO_4^{2-}	2.3	2.1	163.2	23	<.05	225.6	80.8	370.4	409.4	260.3	588.9	1131.8	236.2
NO_3^{-}	0.86	1.21	0.22	0.12	<.02	1.27	0.08	0.07	0.39	0.04	<.01	0.04	0.31
Br^{-}	0.05	0.03	<.02	0.03	<.02	0.06	0.29	0.3	0.11	0.041	0.13	0.2	0.08
Li	0.004	0.004	0.044	0.022	0.038	<0.06	0.105	0.09	-	-	-	-	0.054
B	<0.007	<0.007	0.096	<0.007	0.126	0.33	0.34	0.655	-	-	-	-	0.222
Al	0.042	0.026	0.034	0.034	<.015	-	-	-	-	-	-	-	0.02
Si	23.42	23.49	8.47	9.41	4.41	5.62	4.97	3.96	7.11	7.53	7.58	10.15	4.712
Mn	0.002	0.002	0.006	0.002	0.008	0.005	0.03	0.005	0.01	0.035	0.02	0.01	0.006
Fe	0.008	0.242	0.042	0.008	0.086	0.57	0.95	<0.012	<0.012	0.06	<0.012	0.725	0.034
Sr	0.104	0.082	0.576	0.374	0.296	0.185	0.22	0.565	-	-	-	-	0.228
Ba	0.038	0.018	0.078	0.096	0.046	-	-	-	-	-	-	-	0.02
$\delta^{13}C$ (‰)	-13.97	-13.28	-8.67	-11.32	-7.085	-4.43	-3.08	-3.60	-5.65	-6.84	-5.04	-4.67	-5.986
^{14}C (pmc)	73.33± 0.48	56.45± 0.39	17.84± 0.27	23.96± 0.29	4.61± 0.29	52.29± 0.37	0.74± 0.30	0.28± 0.60	-0.02± 0.30	-0.05± 0.30	-0.14± 030	-0.41± 0.30	-0.14± 0.30
$\delta^{18}O$ (‰)	-10.90	-11.00	-11.55	-11.30	-11.50	-11.20	-11.20	-	-11.9	-11.60	-12.80	-12.70	-12.60
δD (%)	-91.8	-94.5	-94.5	-89.38	-93.87	-98.6	-100.34	-88.5	-97.88	-89.02	-105.42	-105.39	-105.47
Tritium (TU)	<0.8	0.9	<0.8	<0.8	<0.8	<0.8	<0.8	<0.8	<0.8	<0.8	<0.8	<0.8	<0.8
$^{34}S\ SO_4^{2-}$ (‰)	nes	nes	-12.15	-2.25	-6.35	-22.09	-9.95	-8.78	-16.61	-14.55	-18.3	-19.18	-8.89

Values in mg/L unless otherwise noted.
– = not determined; nes = not enough sample; * = bicarbonate values calculated from DIC and pH measurements.

Table 3. Water chemistry data.

Constraints									
C	Na	Ca	K	Al	Si	Mg	S	Cl	Fe

Phases									
Calcite	Ca/Na Exchange	Gypsum	K-spar	Albite	Quartz	Dolomite	Pyrite	Halite	Hematite

Table 4. Elemental constraints and mineral phases specified for geochemical modeling.

			SATURATION INDEX (log IAP/KT)					
Sample	Charge balance error (%)	Alkalinity (meq/L)	**Calcite**	**Quartz**	**K-spar**	**Dolomite**	**Gypsum**	**Albite**
Presbyterian	0.4	1.74	-1.053	1.094	2.446	-2.342	-3.654	0.391
Elkins	-0.8	1.48	-0.568	1.005	1.783	-1.301	-3.776	-0.237
Bibo	-1.6	5.92	0.082	0.533	0.259	0.015	-2.158	-0.298
Seboyeta	-5.8	3.46	-2.67	0.532	0.050	-0.627	-3.013	-0.782
Moquino	7.3	6.70	0.220	0.267	-	0.426	-	-
CNV-W2	3.4	7.71	-0.232	0.348	-	-0.572	-2.670	-
CNV-W3	-1.8	9.66	0.005	0.296	-	-0.505	-2.872	-
CNV-W5	-1.2	9.08	0.681	0.190	-	1.230	-1.833	-
MW-64	11.9	10.56	-0.163	0.473	-	-0.507	-2.159	-
MW-65	-0.9	10.66	-0.117	0.484	-	0.039	-2.236	-
MW-60	-0.7	12.26	0.046	0.499	-	-0.087	-2.063	-
MW-68	-4.3	10.07	0.081	0.627	-	-0.033	-1.692	-
L-Bar	-2.0	7.99	-0.205	0.297	-0.888	-0.583	-2.613	-1.083

- = not calculated due to below detection or unreported values of Al^{3+} (for K-spar and Albite SI) or SO_4^{2-} (for Gypsum SI)

Table 5. Saturation indices (SI) calculated by WATEQF. SI > 0 reflects supersaturation (precipitation expected); SI < 0 reflects subsaturation (dissolution expected).

Sample	Calcite	Quartz	Halite	K-spar	Exchange	Dolomite	Gypsum	Hematite	Pyrite	Albite	^{13}C (‰) computed	^{13}C (‰) measured
Bibo	4.1468	-0.5322	0.3463	-0.0280	3.7707	-0.0690	-0.3900	-0.5162	1.0332	0.0277	-8.679	-8.669
Seboyeta	1.8115	-0.4983	0.1421	-0.0470	1.1570	-0.1311	-0.7145	-0.2324	0.4648	0.0467	-11.345	-11.317
Moquino	4.9482	-0.6725	0.0380	-0.0620	3.4804	-0.1701	-1.5918	-0.3913	0.7839	0.0604	-7.048	-7.085
CNV-W2	6.1373	-0.6294	0.3463	0.0651	6.3281	-0.2091	0.0807	-0.5162	1.1229	-0.0667	-4.504	-4.430
CNV-W5	6.9304	-0.6884	0.2384	-0.0540	7.3562	0.0083	0.4510	-0.8466	1.6931	0.0534	-3.314	-3.300
CNV-W3	8.1745	-0.6524	0.0711	-0.0420	5.0943	-0.2321	-3.1262	-0.9775	1.9720	0.0404	-3.023	-3.080
MW-64	9.0973	-0.5761	0.3154	-0.0119	11.7000	-0.1479	2.5478	-0.5564	0.8482		-5.659	-5.650
MW-65	8.6926	-0.5611	0.8896	0.0072	6.9802	0.1386	-2.0017	-0.4242	2.3458	-0.0088	-6.883	-6.840
MW-60	10.6523	-0.5590	8.5545	-0.0119	11.5841	-0.1479	0.8769	-1.1724	2.6206	0.0103	-5.018	-5.040
MW-68	8.3194	-0.4676	1.1284	0.01224	14.7381	-0.0796	6.0962	-1.3104	2.8456	-0.0138	-4.668	-4.670
L-Bar	6.4312	-0.6635	0.3505	-0.0540	5.8642	-0.2101	-0.6690	-0.7765	1.5534	0.0531	-5.953	-5.986

Table 6. Chemical mass balance transfers generated by NETPATH modeling. Calculations denote the evolution of groundwater chemistry from recharge (as represented by the water chemistry from Presbyterian) to the well location indicated. Mineral units are mmol/kg water. Positive values indicate dissolution and negative values indicate precipitation. Last two columns compare ^{13}C ‰ NETPATH computed values with observed data.

Well	Simple Dissolution Model Corrected ^{14}C age (yr)	NETPATH Corrected ^{14}C Age (yr)	Hydrogeologic Model Calculated Age (yr)
Presbyterian	0	modern	195
Elkins	4360	modern	205
Bibo	2570	2180 ± 120	2415
Seboyeta	4440	3630 ± 100	3355
Moquino	12900	12200 ± 500	19160
CNV-W2	"negative" age	-9300 ± 60	24700
CNV-W3	25200	24000 ± 2800	24650
CNV-W5	33500	33500 ± 9500	24675
MW-64	32000	> 31500	30620
MW-65	32800	> 32800	33110
MW-60	35000	>34500	36175
MW-68	40200	>39900	39670
L-Bar	39100	>38300	63000

Table 7. Groundwater ages calculated from measured ^{14}C activity in groundwater samples using a simple dissolution mass balance and the NETPATH model compared with model-calculated ages.

Geologic Unit	Seepage Velocity Recharge Area (m/yr)	Seepage Velocity Bibo–Cerro Negro (m/yr)	Seepage Velocity Cerro Negro-L-Bar (m/yr)
Two Wells SS	3.90	0.29	0.07 - 0.09
Whitewater Arroyo Sh	0.62 (v*)	0.24 – 0.26 (v*)	0.06 (v*)
Paguate SS	2.93 – 3.69	0.16 – 0.19	0.05
Clay Mesa Shale	0.64 (v*)	0.20 - 0.22 (v*)	0.03
Cubero/Oak Canyon Mb	4.26 – 5.92	0.21	0.11

KEY: v* = vertical flow rate (all other values are horizontal flow rates)

Table 8. Summary of the average groundwater flow rates determined from the calibrated groundwater flow model.

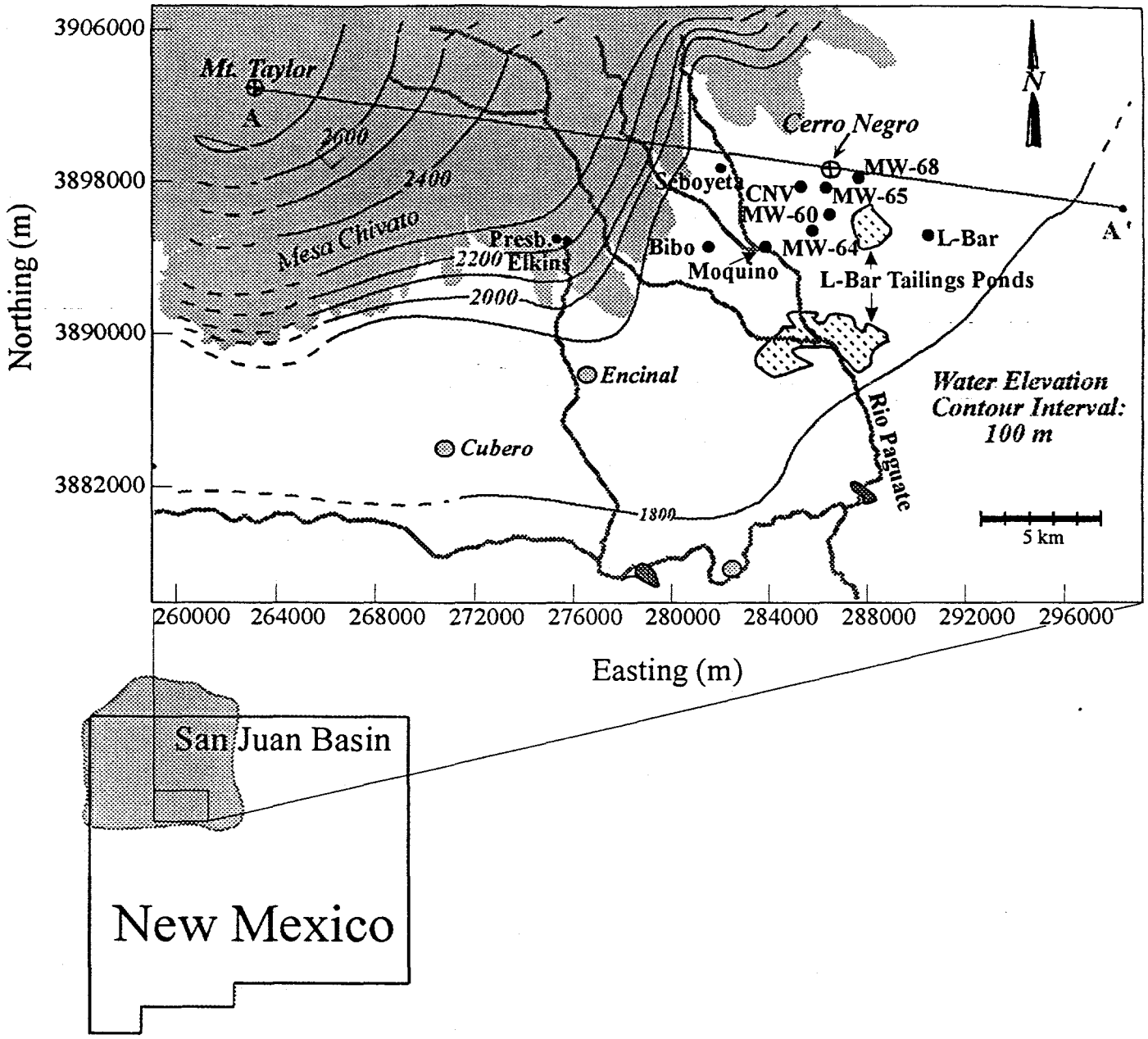

Figure 1. Location of study area in northwestern New Mexico (bottom left); water elevation contour map with groundwater sample locations indicated. A-A' designates the cross-section represented by the model (upper right).

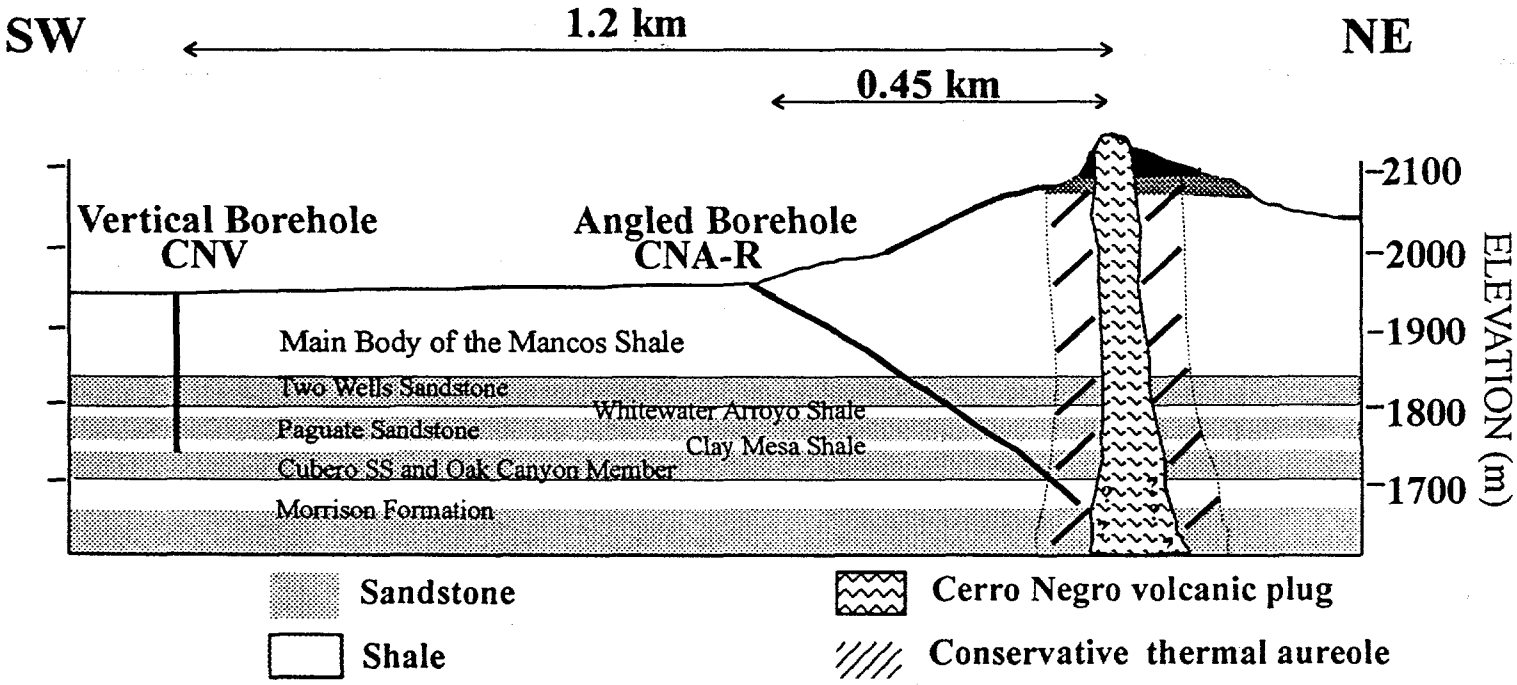

Figure 2. Stratigraphy and orientation of boreholes drilled near the Cerro Negro volcanic neck.

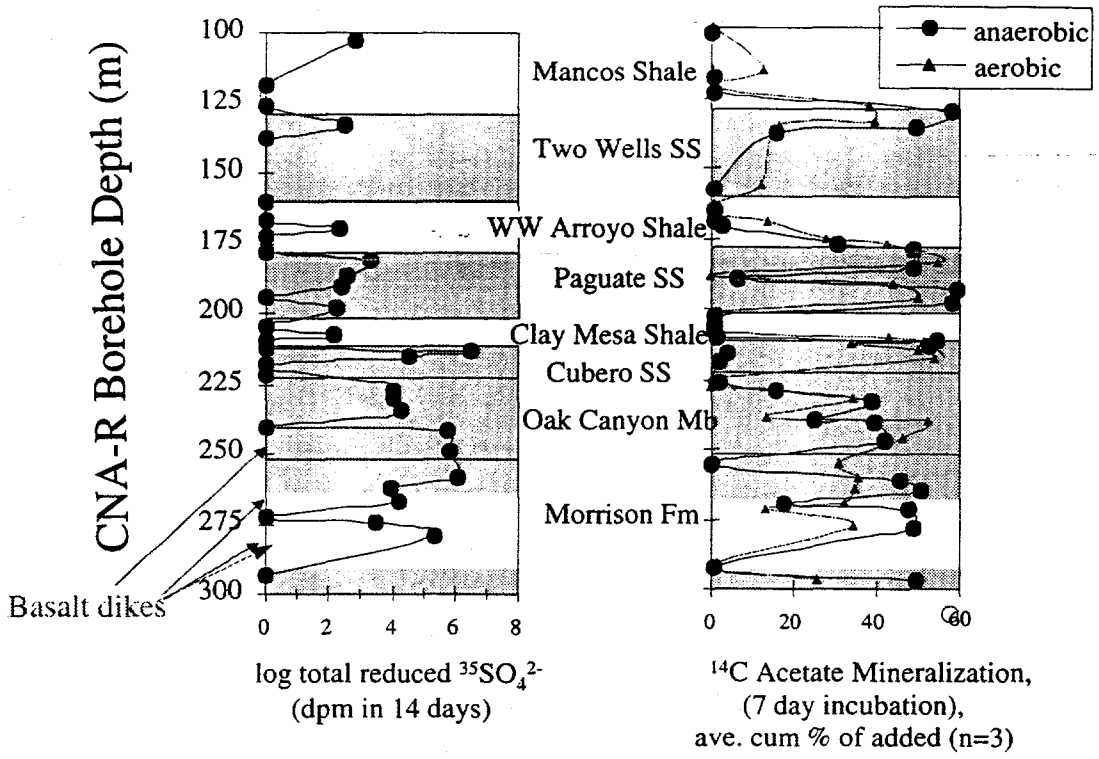

Figure 3. Microbial activity data (total reduced $^{35}SO_4^{2-}$ and ^{14}C mineralization) with depth in the CNA-R borehole. The locations of basalt stringers are noted. In general, higher activities were measured near the shale/sandstone interfaces. Total reduced $^{35}SO_4^{2-}$ and ^{14}C mineralization measurements taken from the vertical borehole (not presented here) showed similar trends, although activities were lower.

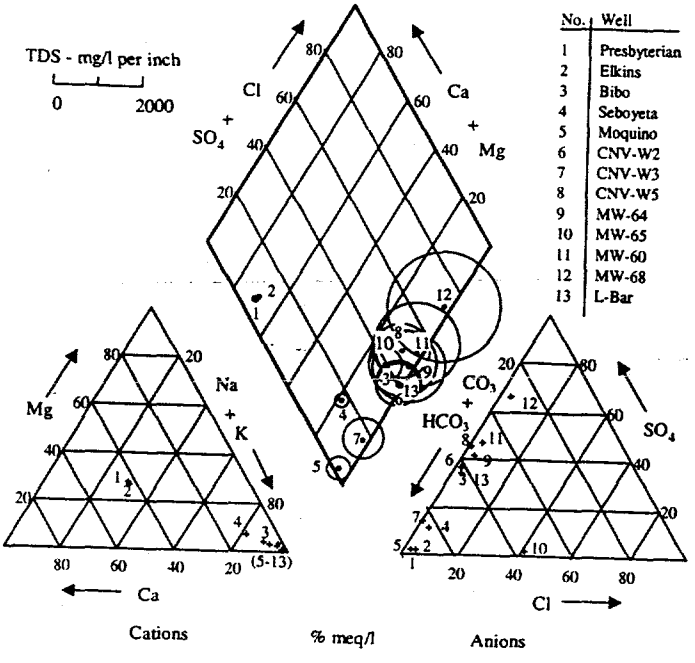

Figure 4. Piper trilinear diagram. The areas of the circles plotted on the central field are porportional to total dissolved solid concentrations for each water sample.

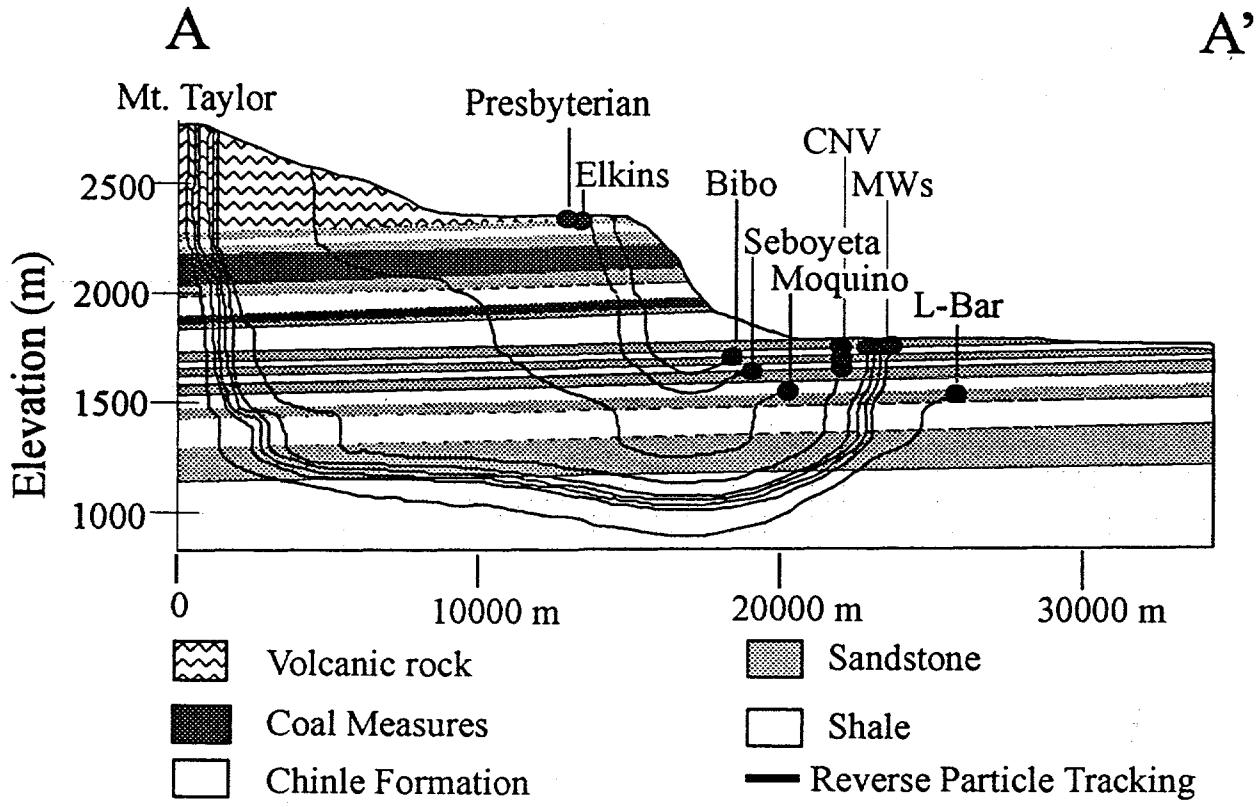

Figure 4. Cross-sectional groundwater flow model, taken from A-A', with well locations and pathlines recorded from reverse particle-tracking. The top boundary represents the water table.

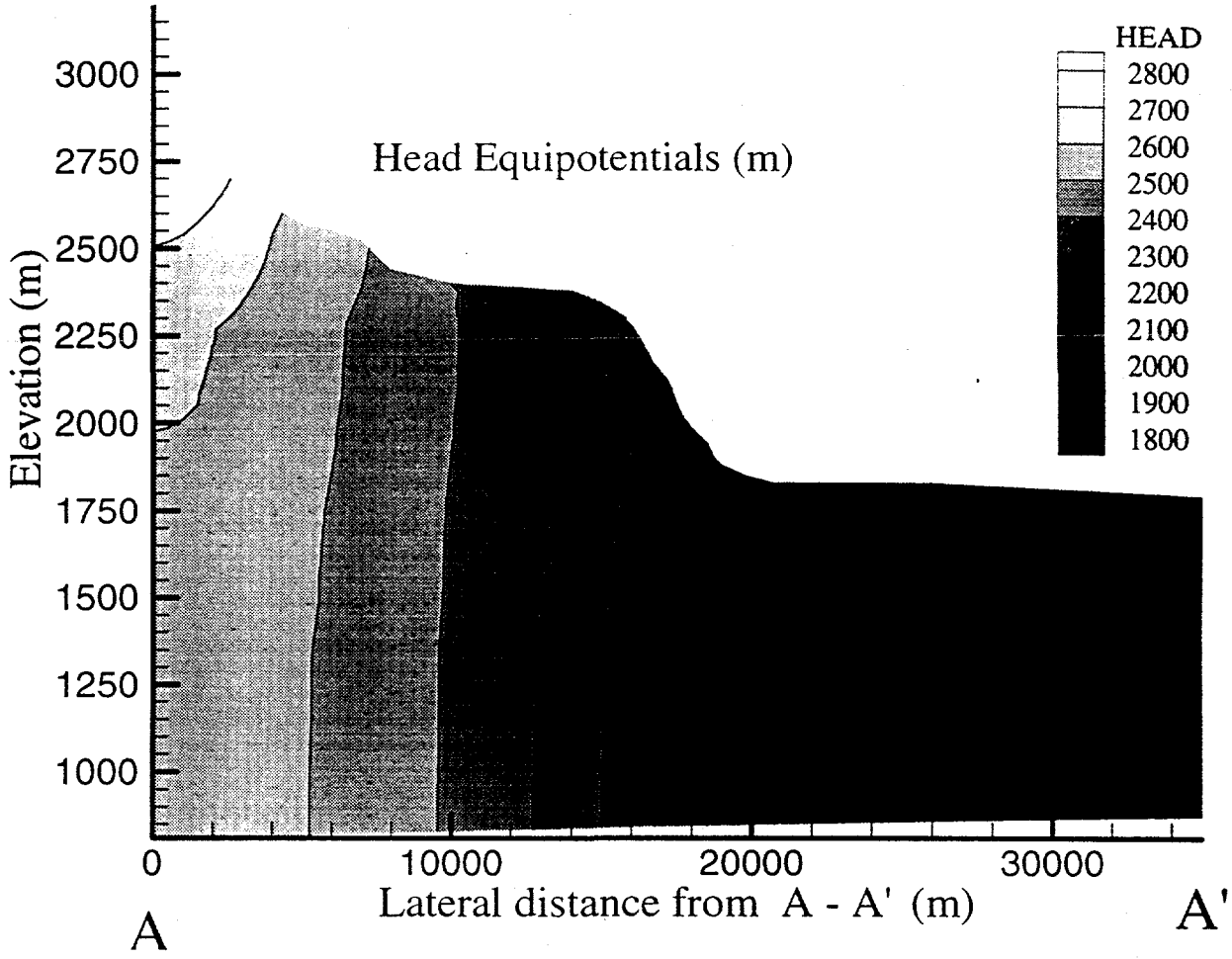

Figure 6. Calculated heads (in m) along cross-sectional transect from Mt. Taylor to east of the Cerro Negro intrusion.

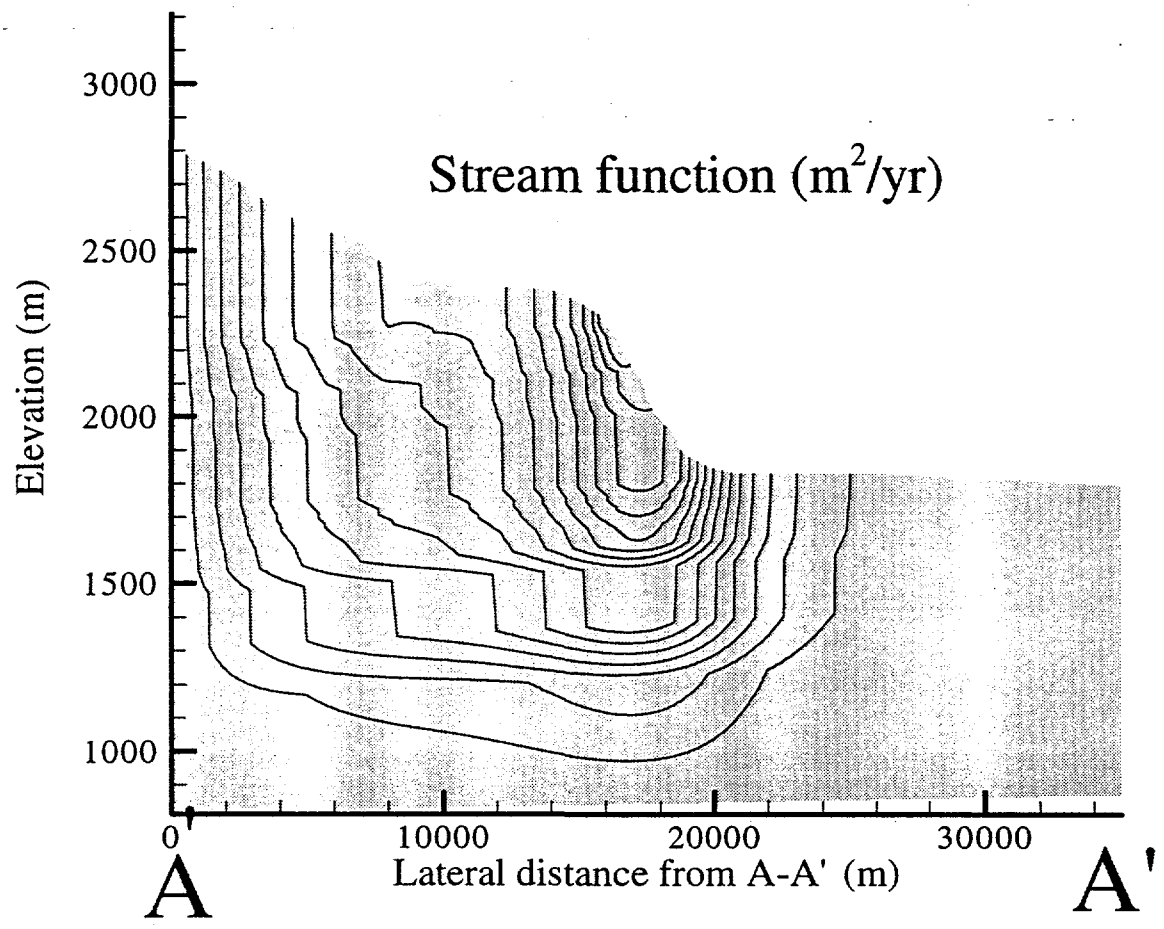

Figure 7. Calculated stream functions (in $m^2\ yr^{-1}$) along cross-sectional transect from Mt. Taylor to east of the Cerro Negro intrusion.

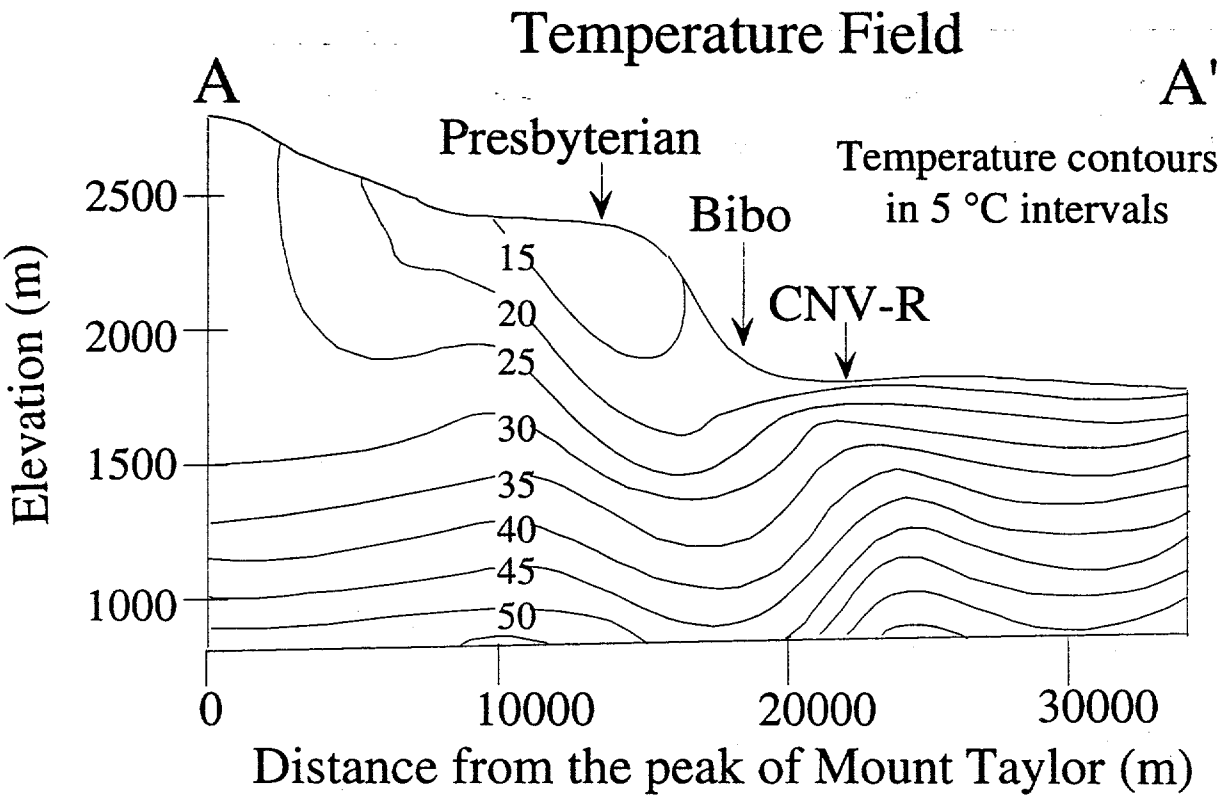

Figure 8. Calculated temperatures (in °C) along cross-sectional transect from Mt. Taylor to east of the Cerro Negro intrusion.

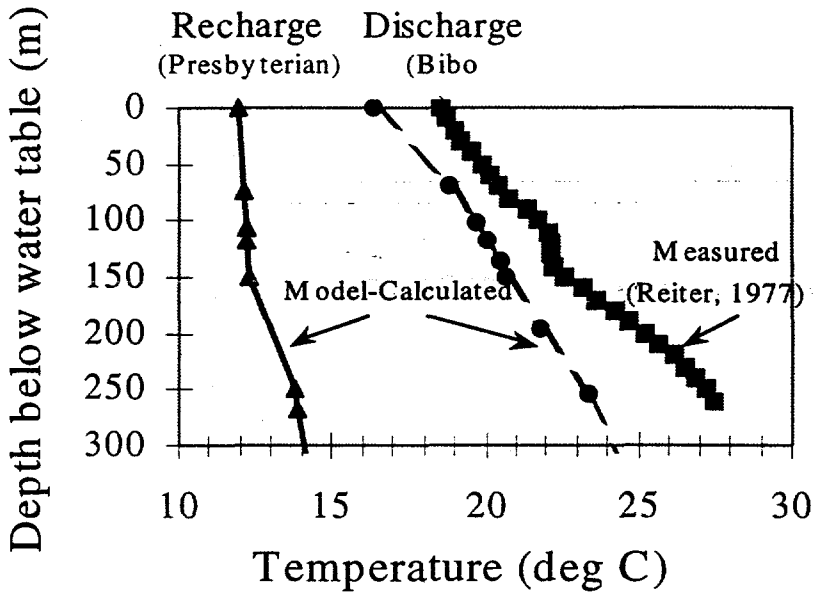
Recharge
(Presbyterian)
Discharge
(Bibo
Depth below water table (m)
0
50
100
150
200
250
300
Measured
(Reiter, 1977)
Model-Calculated
10
15
20
25
30
Temperature (deg C)

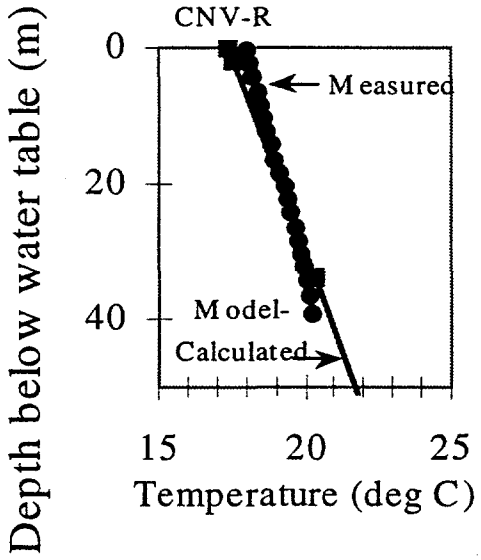
CNV-R
Depth below water table (m)
0
20
40
Measured
Model-
Calculated
15
20
25
Temperature (deg C)